12-14-2013

The role of oxygen in the uptake of deuterium in lithiated graphite

C. N. Taylor
Purdue University

J. Dadras
University of Tennessee

Kara E. Luitjohan
Purdue University, kluitjoh@purdue.edu

Jean P. Allain
Purdue University, allain@purdue.edu

P. S. Kristic
University of Tennessee, Oak Ridge National Lab

See next page for additional authors

Taylor, C. N.; Dadras, J.; Luitjohan, Kara E.; Allain, Jean P.; Kristic, P. S.; and Skinner, C. H., "The role of oxygen in the uptake of deuterium in lithiated graphite" (2013). *Birck and NCN Publications.* Paper 1540.
http://dx.doi.org/10.1063/1.4841115

The role of oxygen in the uptake of deuterium in lithiated graphite

C. N. Taylor, J. Dadras, K. E. Luitjohan, J. P. Allain, P. S. Krstic, and C. H. Skinner

Citation: Journal of Applied Physics **114**, 223301 (2013); doi: 10.1063/1.4841115
View online: http://dx.doi.org/10.1063/1.4841115
View Table of Contents: http://scitation.aip.org/content/aip/journal/jap/114/22?ver=pdfcov
Published by the AIP Publishing

The role of oxygen in the uptake of deuterium in lithiated graphite

C. N. Taylor,[1,a)] J. Dadras,[2,b)] K. E. Luitjohan,[1] J. P. Allain,[1,3] P. S. Krstic,[2,4,5] and C. H. Skinner[6]
[1]*School of Nuclear Engineering, Purdue University, West Lafayette, Indiana 47907, USA*
[2]*Department of Physics & Astronomy, University of Tennessee, Knoxville, Tennessee 37998, USA*
[3]*Birck Nanotechnology Center, West Lafayette, Indiana 47907, USA*
[4]*Joint Institute of Computational Sciences, University of Tennessee, Knoxville, Tennessee 37998, USA*
[5]*Physics Division, Oak Ridge National Laboratory, Oak Ridge, Tennessee 37831, USA*
[6]*Princeton Plasma Physics Laboratory, Princeton, New Jersey 08543, USA*

(Received 19 September 2013; accepted 20 November 2013; published online 10 December 2013)

We investigate the mechanism of deuterium retention by lithiated graphite and its relationship to the oxygen concentration through surface sensitive experiments and atomistic simulations. Deposition of lithium on graphite yielded 5%–8% oxygen surface concentration and when subsequently irradiated with D ions at energies between 500 and 1000 eV/amu and fluences over 10^{16} cm^{-2} the oxygen concentration rose to between 25% and 40%. These enhanced oxygen levels were reached in a few seconds compared to about 300 h when the lithiated graphite was allowed to adsorb oxygen from the ambient environment under equilibrium conditions. Irradiating graphite without lithium deposition, however, resulted in complete removal of oxygen to levels below the detection limit of XPS (e.g., <1%). These findings confirm the predictions of atomistic simulations, which had concluded that oxygen was the primary component for the enhanced hydrogen retention chemistry on the lithiated graphite surface. © *2013 AIP Publishing LLC*. [http://dx.doi.org/10.1063/1.4841115]

I. INTRODUCTION

Lithium has reached a pervasive position as an advanced material interface in novel applications including: solid-state batteries, hydrogen storage, reactive fuel cells, and nuclear magnetic fusion plasma-facing materials.[1–3] In many of these systems, it is lithium's unique relationship with hydrogen that provides advanced performance. Lithium has also had a historical impact in its use in nuclear reactor systems including fission and fusion applications. Recently, lithiated carbon has emerged as an attractive plasma-facing material in magnetic fusion devices.[4] Lithium's low ionization energy (~5.4 eV), low heat of evaporation, and high sticking coefficient make it an excellent plasma-facing surface with very low risk of contaminating the core plasma.[5] In tokamaks, hydrogen isotopes (i.e., deuterium and tritium) are the primary fuel and their interaction with the device walls is critical in determining fusion reactor performance. The average incident particle energy of D and T particles at the walls varies between 10 and 200 eV/amu. Under these conditions, the penetration depth is below 10 nm. Therefore, the large-scale fusion plasma is, in principle, dominated by a very thin surface layer at the plasma-wall interface. Deciphering the physical chemistry between hydrogen and lithium-based surfaces, and correlating it to the performance of these fusion devices has been challenging. This lack of understanding is primarily a result of the extreme, far-from-equilibrium[6] conditions to which these material's surfaces are exposed.

Lithium wall coatings have improved plasma performance on a number of fusion devices including TFTR,[7] CDX-U,[8] FTU,[9] TJ-II,[10] T-11M,[11] EAST,[12] and NSTX.[5] These improvements have come via a reduction in deuterium recycling in addition to a reduction in oxygen and carbon impurities in the plasma. In other words, plasma performance improves due to deuterium uptake and this uptake is enhanced with lithiated graphite. Thus, conditioning the walls of magnetic nuclear fusion devices with low-doses of about 100–1000 nm equivalent lithium thin-film thickness has been correlated with a substantial improvement in the plasma energy confinement time. Initially, experimentalists began studying lithium in its liquid state undoubtedly with hopes of maintaining a pure and controllable surface to simplify interpretation of the results.[13] These studies enhanced understanding of plasma-surface interactions with lithium and led to the conjecture that deuterium binds with pure lithium by forming lithium-deuteride (LiD). As a result, these findings have been freely extrapolated to environments where lithium is present with other species, such as lithiated graphite in fusion devices. This paper is an extension of recently published work by Krstic *et al.* that demonstrated the importance of complex interactions between lithium and graphite substrates with enhanced oxygen surface concentrations and their effect on the increased deuterium uptake and suppressed carbon erosion.[14] Here, we solidify and fully validate these findings by extensive experimental study which shows the mechanisms for accumulating oxygen at the surface of the lithiated graphite.

Lithiated graphite exhibits a complex and rich surface chemistry. X-ray photoelectron spectroscopy (XPS) of virgin ATJ graphite (cut and polished, but in an otherwise unaltered state) reveals two spectral peaks at 284.5 eV and 532 eV that

[a)]Author to whom correspondence should be addressed. Electronic mail: chase.taylor@inl.gov. Present address: Fusion Safety Program, Idaho National Laboratory, Idaho Falls, Idaho 83415, USA.
[b)]Present address: Department of Chemistry & Biochemistry, University of California Los Angeles, Los Angeles California 90095, USA.

correspond to C(1s) and O(1s) core electrons, respectively, as shown in Figure 1. On average, oxygen accounts for ~5% of the atomic surface concentration. Evaporating lithium onto the graphite also readily introduces Li-O interactions in the form of oxides, super-oxides, and peroxides.[15]

After depositing a 2-μm lithium dose, the lithium immediately begins to bind with oxygen present in the graphite, and in addition, adsorbs oxygen from the ambient vacuum ($<10^{-9}$ mbar in laboratory experiments).[16,17] Unlike depositing lithium films on a flat impermeable substrate, lithium promptly intercalates into graphite.[17–20] Furthermore, multi-scale micron and nanometer sample roughness increases the sample surface area resulting in further deviation from the nominal lithium dose that would be deposited on a perfectly flat surface.[14]

Depositing lithium typically increases the oxygen surface concentration by a factor of two (up to ~10% oxygen concentration) within 30 min following lithium deposition. Subsequent deuterium bombardment further increases the surface oxygen concentration to relative amounts reaching 40% in some samples. Deuterium bombardment results in additional chemical interactions which are visible in both the O(1s) and C(1s) photoelectron ranges from XPS data in Figure 1. These resultant Li-O-D and Li-C-D interactions only appear when exposing lithiated graphite to deuterium bombardment. The analyses exploit an indirect method of observing deuterium interactions on lithiated graphite since deuterium atoms do not emit sufficient photoelectrons to be detected via XPS. Further details can be found in previous publications.[17,21]

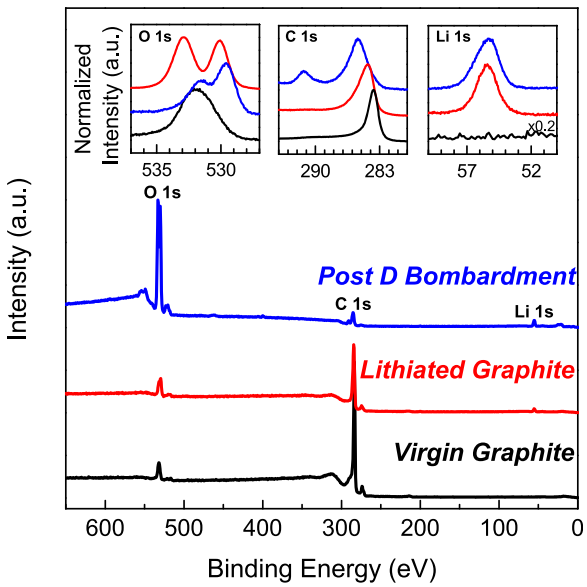

FIG. 1. X-ray photoelectron spectra of lithiated graphite. Un-treated "virgin" graphite (black) has two primary photoelectron peaks whose binding energies are characteristic of the presence of carbon C(1s) (~284 eV), and oxygen O(1s) (~532 eV). Depositing lithium (red) on virgin graphite results in the formation of a second peak in the O(1s) region (detail shown in O(1s) inset), which is indicative of new chemistry. Deuterium ion bombardment (blue) of lithiated graphite results in further enhanced chemistry in the O(1s) energy range as well as the formation of a new peak (i.e., new chemistry) observable in the C(1s) region (291.2 eV). The latter peaks represent deuterium-oxygen and deuterium-carbon bonds that are catalyzed by the presence of lithium on graphite. Furthermore, oxygen surface concentration of the lithiated graphite is greatly increased by deuterium bombardment.

Figure 2 shows the mean oxygen concentration after deuterium irradiation for eight samples at various stages. Six of the samples had a nominal lithium dose of 2 μm deposited. The variance in the data is a result in part due to the intrinsic surface morphology of the ATJ graphite samples. In the context of this paper, this issue is not examined and left for future work. As one would expect, the reactive and electronegative nature of lithium attracts oxygen and modestly increases the oxygen surface concentration. Deuterium ion bombardment further increased the oxygen concentration. Interestingly, irradiating the two samples where lithium was not deposited (triangles) actually depletes the oxygen surface concentration.

The startling result from Figure 2 is that the oxygen concentration increases dramatically during deuterium ion irradiation. Ion bombardment triggers a dynamic mechanism that drives oxygen within the probing depth of XPS (<8 nm). Moreover, there is a non-trivial oxygen concentration in the deposited lithium. Potential oxygen sources and their contribution to the oxygen surface concentration is convoluted and is the focus of current investigations.

In this follow on of recently published work,[14] the primary objective is to expand our understanding of oxygen surface evolution and to detail its correlation to deuterium retention from our recent atomistic simulations and *in-situ* surface characterization of lithiated graphite exposed to low-energy deuterium ions. In particular, we investigate the dramatic enhancement of oxygen accumulation on the lithiated graphite surface and its role on deuterium retention. The studies here focus on the *dynamic* behavior of irradiated lithiated graphite under conditions both in thermodynamic equilibrium and far-from thermodynamic equilibrium (resembling extreme conditions such as plasma irradiation in fusion devices). Specifically, in Sec. III A we consider the

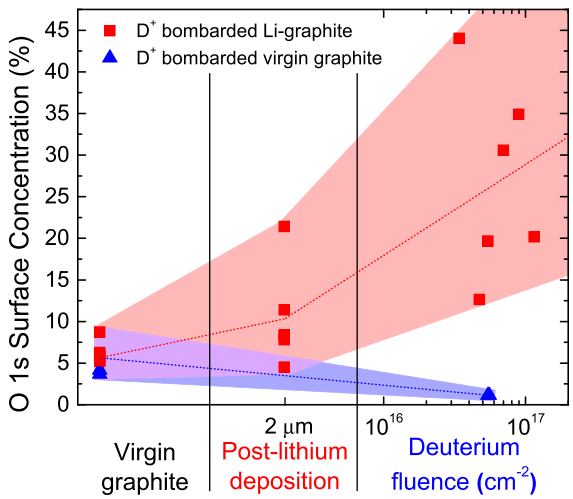

FIG. 2. Oxygen surface concentration after deuterium irradiation with and without lithium pre-conditioning. The x-axis represents experimental steps and connecting lines are shown to track individual samples. The dotted lines represent the average oxygen concentrations for the two processes and the wide bands represent the extent of scatter in the data.

oxygen concentration (1) as a function of time following lithium deposition, (2) as a function of lithium dose, and (3) as deuterium irradiation fluence increases. Atomistic simulations are discussed in Sec. III B and confirm deuterium retention is primarily due to the oxygen within the simulated matrix. The implications of this work directly affect wall-conditioning techniques in nuclear fusion devices, as well as lithium-based systems used in hydrogen storage, lithium batteries, and semiconductor development.

II. EXPERIMENTAL SETUP

A. Equipment and techniques

Experiments were conducted in the PRIHSM (Particle Radiation Interaction of Hard and Soft Matter) and Omicron facilities in the Birck Nanotechnology Center (BNC) at Purdue University described in detail in Refs. 17 and 22, respectively. GrafTech ATJ graphite samples are cut, mechanically polished, and used in all experiments. In both facilities, lithium evaporation is achieved using a custom-built thermal evaporator. Lithium deposition rate is measured using a quartz crystal microbalance (QCM) and nominal lithium film thickness has been cross calibrated using cross sectional scanning electron microscopy showing a 6% error in depositing a 2 μm film. Evaporating lithium on graphite, however, does not result in epitaxial films due to intercalation[17,19] and substrate surface morphology; therefore, lithium depositions are referred to as nominal doses. Ion irradiation is typically conducted at 1000 eV, but ion energy, flux, and fluence vary according to experimental requirements. A quadrupole mass spectrometer with a line-of-sight collection of emitted species during irradiation measures the ion-induced emission from the irradiated samples surface. Coupling the QMS data with XPS data taken *in-situ*, the effect of any contamination from either the evaporation or irradiation sources can be determined. A separate experiment used two different substrates to assess the effect of contamination from the low-flux, low-energy ion source. First, a material sample, GaSb, with high affinity for oxygen was used. The native oxide layer was measured by analyzing the Sb-4d and Ga-4d peaks. The irradiation with Ar+ ions yielded a nominal $10^{16}\,cm^{-2}$ fluence to remove the thin native oxide layer with no sign of an *increase* in the oxide suggesting any ion-gun induced impurity. Further, a GaSb sample with no native oxide layer was also irradiated. This also resulted in no oxide formation. A gold sample was also irradiated and both XPS and LEISS used to measure any sign of ion-beam contamination from three different ion-based sources. None of the irradiations yielded any sign of oxide formation on the surface during irradiation. Fluence dependence was measured by sequence of identical irradiations, with intermittent analysis performed between irradiation steps. Nominally, deuterium irradiation consists of a beam with about 75% D_2 and 25% D composition. Therefore, energies can range between less than 100 eV/D up to 500 eV/D. Previous studies found that the surface chemistry is independent of implantation energy.[14]

XPS uses a dual anode, non-monochromatic X-ray source where Al Kα anode is selected when analyzing lithiated graphite.[23] Photoelectron energy is analyzed using a VG Scienta hemispherical analyzer. Scofield cross sections[24] are used to determine relative sensitivity factors for quantifying relative atomic concentrations using the CasaXPS software. In calculating atomic surface concentrations, educated objectivity based on the spectrum peaks and any *a priori* knowledge of the sample is use in determining which elements should be included in the analysis. The sum of each surface concentration from individual constituents is constrained to equal 100%. Occasionally, multiple peaks are contained within a single elemental characteristic photoelectron energy range (e.g., the two peaks in the O(1s) range after deuterium bombardment). In these instances, the surface concentration is the sum aggregate of all peaks within that range. Due to the low probability of electron emission, deuterium cannot be detected directly using XPS. Instead, deuterium must be examined indirectly as it interacts with other species, such as oxygen, thus providing a useful technique for examining deuterium retention chemistry.

B. Surface conditioning

Physical vapor deposition of metals typically results in layer film growth on the substrate. Lithium deposition on graphite, however, does not fit this representation for two primary reasons. First, lithium and other alkalis intercalate into graphite (as well as other carbon allotropes). The second reason consists of the substrate morphology. Epitaxial thin-film growth is generally associated with deposition of ultra-smooth films, such as in semiconductor device applications. The result is that most films are grown on relatively flat substrates. The graphite used in the experiments discussed throughout this paper is mechanically polished, yet still has micron and nano-scale roughness as illustrated and shown in Figure 3.

The graphite used in fusion devices typically is not polished and roughens significantly throughout an experimental campaign due to plasma bombardment. During plasma exposure, carbon atoms are displaced from their lattice sites and the surface quickly becomes amorphized. In addition, sputtered carbon redeposits on surfaces throughout the device. Consequently, surface area increases with roughness, which effectively prevents the deposited lithium from building a complete epitaxial film on top of the graphite tile surface. These two phenomena illustrate that it is more accurate to quantify lithium depositions as a "dose" or "nominal thickness" rather than a "thickness" as obtained on a flat surface. Therefore a "1 μm" deposition quoted in this work is associated with a dose of $4.63 \times 10^{18}\,cm^{-2}$ lithium atoms (assuming a flat surface with an area of 1 cm^2 and lithium density of 0.534 g/cm^3).

III. RESULTS AND DISCUSSION

A. Oxygen surface concentration dependence on lithium conditioning of ATJ graphite

Our previous work[14] considered deuterium evolution during hydrogen bombardment of oxidized and lithiated graphite. Here, we study the parameters, which influence the surface concentration of oxygen in the lithiated graphite surface. Specifically, in this section, we consider the oxygen

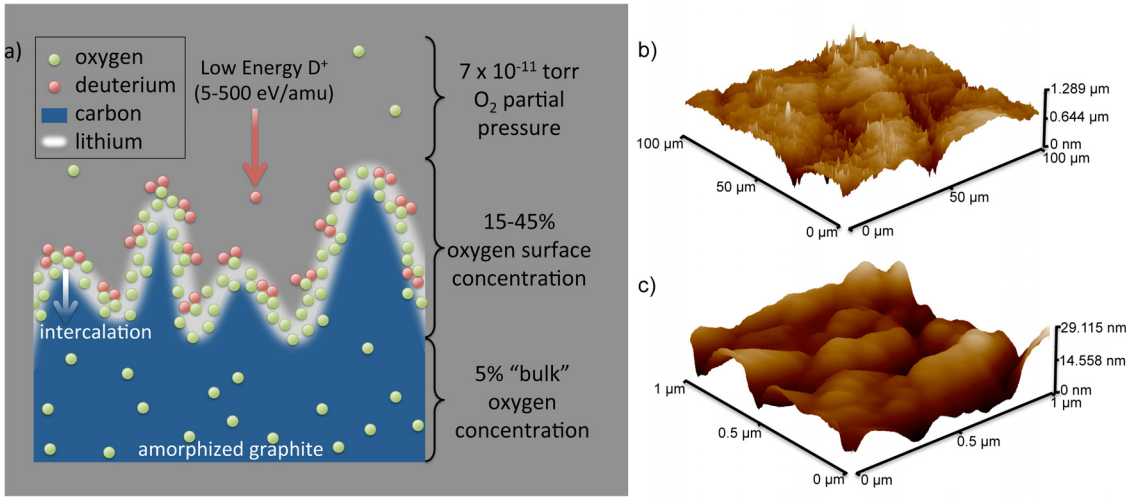

FIG. 3. Illustration of the dynamics in lithiated graphite. Polished graphite samples have surface height variations of $>1\,\mu$m (for a $100 \times 100\,\mu$m domain) in addition to local height variations on smaller domains, as shown in the inset atomic force micrographs (AFM) in (b-c). When depositing lithium films on such rough surfaces, the effective film "thickness" is significantly less than the nominal dose due to the increased effective surface area. Furthermore, lithium rapidly intercalates into graphite following deposition. Highly electropositive lithium (0.95, Pauling[25]) attracts electronegative oxygen (3.4, Pauling) from the polished graphite ($\sim$6% O_2 concentration) as well as from the ambient vacuum (O_2 partial pressure of $\sim 10^{-11}$ mbar during lithium deposition). Lithium deposition causes a modest average rise in surface oxygen concentration to approximately 10%. For some samples, experiments show that deuterium ion bombardment dramatically increases the surface oxygen concentration to as much as 45%.

concentration as a function of (1) time after deposition, (2) lithium dose, and (3) deuterium fluence.

1. Time after deposition

The sequence of surface treatment typically begins with lithium evaporation on graphite followed by ion irradiation. Evaporating lithium onto virgin graphite immediately initiates two phenomena: intercalation and oxygen adsorption (gettering). Intercalation in the context of fusion wall conditioning has been studied elsewhere in extensive detail.[15,18,19] Intercalation consists of lithium diffusing away from the surface to regions between graphite basal planes. Concurrently, upon deposition, the lithium begins to getter ambient oxygen. Lithium gettering[26,27] can be partially described by considering the electronegativity of lithium and oxygen. Lithium has a low electronegativity (0.94 Pauling-scale) and readily polarizes in the higher electronegativity environment (carbon, 2.4, hydrogen, 2.2, oxygen 3.4,[20]), thus attracting highly electronegative oxygen.[28] Even in ultra-high vacuum (UHV), residual oxygen can oxidize the lithium surface.[29]

Three graphite samples remained in UHV ($\sim 10^{-10}$ mbar) for nearly 2 weeks following lithium evaporation. During this period, XPS was performed periodically and the surface concentrations were quantified as presented in Figure 4. The average oxygen concentration of the virgin graphite samples was $5.4 \pm 0.4\%$. An exponential fit applied to the data suggests a possible trend. Over the course of up to 300 h, the average oxygen concentration increased above 20%. This diffusion-limited process relies on the surface achieving thermodynamic equilibrium with the ambient vacuum. Exposure to $\sim 10^{-10}$ mbar for 100 h corresponds to $\sim$36 Langmuirs (where 1 Langmuir is defined as an exposure of 1×10^{-6} Torr (1.33×10^{-4} Pa) for 1 s). This corresponds well to Ref. 29 where lithium within the probing depth of XPS was found to oxidize between 20 and 40 Langmuirs.

2. Lithium dose

Initial laboratory studies used 2 μm lithium doses as this number approximated the mid-cycle average accumulated lithium dose during a NSTX lithium campaign. Since a given lithium dose gradually increases, the oxygen concentration as shown in Sec. III A 1, we tested smaller lithium doses to determine if they would have a lesser gettering effect than larger lithium doses. Nominal lithium doses of 50, 100, 1000, 2500, and 5000 nm were deposited on separate ATJ graphite samples with XPS performed prior to and following

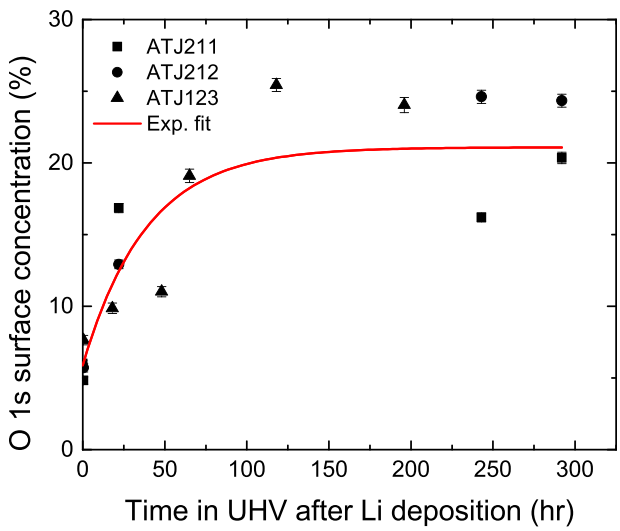

FIG. 4. The oxygen surface concentration of lithiated graphite slowly increases from $\sim$5% to more than 20% as the samples sit in 10^{-10} mbar UHV over the course of 100 s of hours. The exponential fit of the adsorption behavior is representative of the Langmuir isotherm, where the oxygen surface coverage θ approaches a steady-state concentration dictated by a localized thermodynamic equilibrium.[30] Error bars represent computational propagation of uncertainty in surface quantification.

lithium deposition. The oxygen surface concentration before and after lithium depositions was calculated and shown in Figure 5. Surprisingly, in the absence of irradiation, the prompt surface oxygen concentration is not clearly linked to lithium dose.

Other gettering systems have shown a strong dependence on surface porosity, morphology, and consequently surface area.[31] Since the graphite samples used in the present experiments were prepared identically, each has a nominally equivalent surface area for adsorbing oxygen ($\sim$1 cm^2). After lithium deposition, regardless of lithium dose, each sample oxidizes at a rate proportional to its surface area. The large observed variations in Figure 5 outside of the error bars can be attributed to variations in surface roughness and deviations in the time elapsed between lithium deposition and XPS ($\sim$30 min for each sample).

3. Deuterium fluence

Figure 2 showed the oxygen concentration of many samples after a prescribed lithium and deuterium dose, and in each case, the oxygen concentration increased most dramatically during deuterium irradiation. In order to resolve time dependence of the oxygen uptake during deuterium irradiation, we performed XPS at much shorter fluence intervals. Figure 6 shows the fluence-dependent oxygen concentration during D^+ bombardment. After deposition of a nominal lithium dose of 2 μm, the oxygen concentration was about 6.0%. Subsequently, the lithiated graphite sample was bombarded with deuterium ions for 1 min (3.9×10^{15} cm^{-2}). After this 1 min irradiation, the oxygen concentration increased to 21.3%! Advancing the irradiation an additional 1 min, to a cumulative fluence of 8.2×10^{15} cm^{-2}, further increased the surface oxygen concentration to 27.3%. Irradiation incrementally continued to a total fluence of 5×10^{17} cm^{-2} (2 h) and the oxygen surface concentration peaked at 40.4%. Surface impurities were taken into consideration but did not have a significant contribution, where nitrogen reaches a maximum concentration of 2.8%.

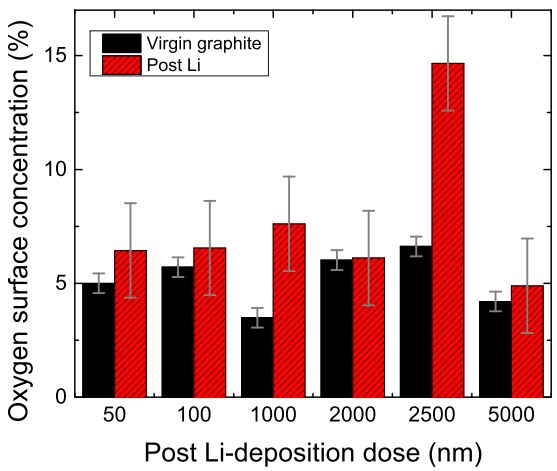

FIG. 5. Surface oxygen concentration for nominal lithium doses of 50, 100, 1000, 2000, 2500, and 5000 nm deposited on separate ATJ graphite samples. The data indicates that prompt gettering rate is more strongly influenced by surface area than lithium dose. Error bars represent computational propagation of uncertainty in surface quantification.

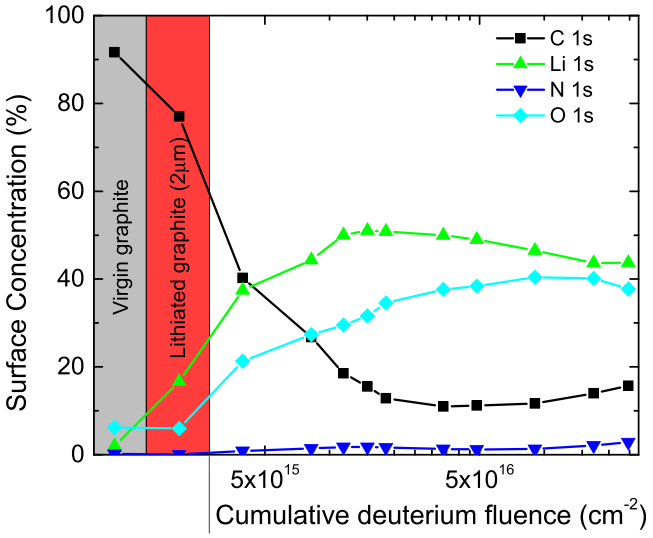

FIG. 6. Oxygen concentration during 500 eV/amu deuterium bombardment. Data points in the left-hand gray panel represent the graphite sample in its virgin state; data in the adjacent red panel are taken after depositing lithium. Next, a 1-min irradiation commenced (3.9×10^{15} cm^{-2}) and increased the oxygen surface concentration from 6.0% to 21.3%. Subsequent irradiation steps further increase the oxygen surface concentration to 40.4%.

The time scales required to increase the surface oxygen concentration to $\sim$20% in Figures 4 and 6 are striking. A 1 cm^2 sample has $\sim 5.4 \times 10^{16}$ atoms within the probing depth of XPS (assuming a probing depth of 5 nm). The increase from 6% to 21% during a 1 min irradiation corresponds to an oxidation rate of $\sim 5 \times 10^{17}$ atoms/hour, or monolayer coverage in 1.16 min. In Figure 4, with an O_2 partial pressure of $\sim 5 \times 10^{-10}$ mbar, the oxygen-surface collision rate is 1.8×10^{11} cm^{-2}s^{-1}. At this rate, it would take approximately 2 h to achieve monolayer coverage, assuming the substrate has 1.3×10^{15} initial surface sites, 1:1 uptake efficiency, and the sample and chamber are at room temperature.[32] Contrasting these two mechanisms, the ion-induced oxygen enhancement is about 100 times faster than ambient oxygen adsorption.

Interestingly, the Li 1s concentration increases along with the O 1s signal during the beginning of the deuterium irradiation sequence. This indicates that irradiation drives lithium and oxygen to the surface. The precise mechanism responsible for this phenomenon is unclear and is under investigation. It should be noted that the quantification software constrains the sum total of all surface concentrations to equal 100%. Therefore, the rise in the oxygen and lithium concentrations, for example, must correspond to a decrease in another constituent (e.g., carbon). After depositing a nominal lithium dose of 2 μm, one would expect the carbon to become buried and not detectible through XPS. The graphite surface morphology effectively thins the deposited lithium and intercalation rapidly diffuses lithium into the graphite (see Figure 3 and surrounding discussion).

Although oxygen is found to vary dramatically in Figure 6 as well as in the previous sections, XPS cannot conclusively isolate the enhanced deuterium retention to the increased oxygen concentration. Atomistic simulations are particularly useful since matrices that are difficult or

impossible to prepare in the laboratory can be simulated (i.e., carbon and lithium without any oxygen). Accordingly, matrices of pure carbon, carbon with only lithium, carbon with only oxygen were modeled and the results are presented in the following section.

B. Molecular dynamics simulations of deuterium binding chemistry in lithiated graphite bombarded by deuterium

Atomistic simulations of the Li, C, O, and D system show that oxygen is the preferred channel for deuterium binding.[14] The details of these simulations were not included in our previous work,[14,28] but are presented herein. We also present new analyses that strengthen our previous conclusions.

The equilibrium partial charges of the atoms that take part in polar interactions between hydrogen and other matrix materials depend on coordinates of all atoms in the system. The coordinates typically change in each simulation step, enforcing a need to accurately calculate the charge dynamics during the system evolution. Semiempirical methods such as the Electronegativity Equalization Method (EEM),[33] besides having questionable accuracy, might put an unreasonable time lag on calculations with classical molecular dynamics.[34] We chose a quantum-classical molecular dynamics approach,[35] treating nuclei of the system as classical particles but performing adiabatic quantum mechanical calculations for electronic motion at each time step. Note that lithium has a very low electronegativity ($\sim$0.94, on the Pauling scale[25]), in comparison to hydrogen (2.2), carbon (2.4), and oxygen (3.4). In effect, in the process of binding, lithium will easily become electropositive and oxygen electronegative while hydrogen and carbon will find their place somewhere in between.

The critical issue in our approach is the solution of the Schrodinger equation for valence electrons of the system in each time step (1 fs). We employ the Self-Consistent-Charge Density Functional Tight Binding (SCC-DFTB) method, developed by the Bremen Center for Computational Material Sciences.[36,37] This is an approximation to Density Functional Theory (DFT), in which only valence orbitals and a minimal basis set are considered and the difficult density integrals are parameterized and fitted in advance. Thus, the method is faster, up to 10^3 times, than first principles DFT, fitting well into the range of the current computational capabilities. The DFTB pair-parameters for the Li-C-O-H system developed by Maeda and Morokuma in 2010 (Refs. 14 and 28) were employed. This method was adapted for high throughput Monte Carlo calculation of 5004 random trajectories on the petascale supercomputer environment[28] using embarrassing parallelization (one core per trajectory). Using 5004 processors at the Kraken Cray xt5 computer, the calculation required more than 30 000 CPU hours per mixed system matrix, with 264 atoms per matrix. The trajectories have a random point of impact at the simulation surface interface, otherwise they are initially parallel. The impact energy of the deuterium atoms is 5 eV, being limited by the size of the simulation cell, i.e., the number of atoms considered in this quantum-classical approach. However, as illustrated by experiments in Ref. 14, qualitatively, this does not influence the studied uptake results, which is determined by the binding chemistry of deuterium. The chemistry evolves when the impact cascade almost thermalizes with the surface environment, irrespective of the deuterium impact energy.

The histogram in Figure 7 presents the resulting integrated distribution of retained deuterium nearest neighbors. The table in Figure 7 summarizes the compositions of five different simulations matrices used for deuterium bombardment. Notably, 20% lithium in carbon (Matrix Q) leads to only 9% of lithium-deuterium nearest neighbors. In contrast, a matrix comprised with 20% oxygen in carbon leads to 30% of oxygen-deuterium nearest neighbors. Matrix R is comprised of 20% oxygen and 20% lithium, and results in deuterium having 27% oxygen and 5% lithium as its nearest neighbor. Thus, when oxygen is present in the matrix, deuterium prefers to be near oxygen rather than lithium. The prominence of carbon nearest neighbors is a result of its ability to retain deuterium,[38] and its large atomic concentration in the prepared matrix. Future simulations will test matrices with trace concentrations of carbon and oxygen in lithium in order to quantify the role of carbon-oxygen retention.

The conclusions in Figure 7 are obtained through a "nearest neighbor" analysis in Figure 8, which assumes that binding is more likely to occur between two neighboring atoms rather than distant atoms. Accordingly, we determined the final rest location of the deuterium projectiles in relation to other elements in the matrix and tabulated the nearest neighbors of the D atom. Even when there is an equal quantity of O and Li in the carbon, as seen in Figure 8 case R (e) and (f), the oxygen by far dominates as the nearest bonding neighbor where >20% of the implanted deuterium ions have oxygen as their closest neighbor and <5% have lithium. In case T (i,j), where the carbon matrix is void of lithium and has 20% of oxygen, implanted deuterium atoms have oxygen

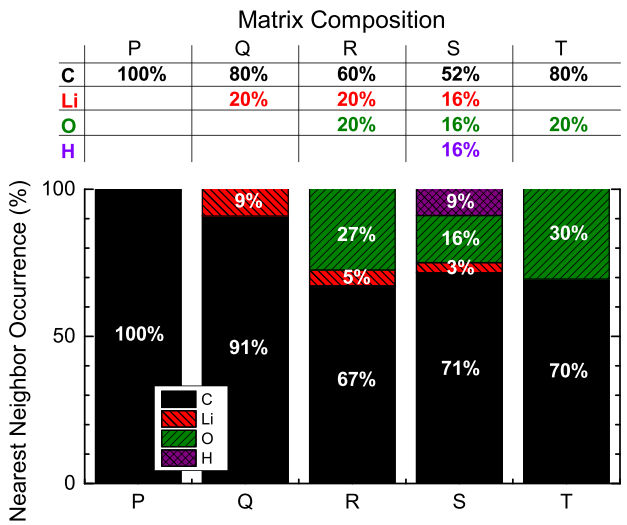

FIG. 7. The composition of each matrix used as input in the simulations is shown in the table. The results of the simulation are shown in the histogram. The percent-integrated distribution of deuterium nearest neighbors after deuterium ion bombardment for various matrix compositions is reported. When oxygen is present in the matrix, it becomes the predominant nearest neighbor to deuterium, an indication of binding pairs.

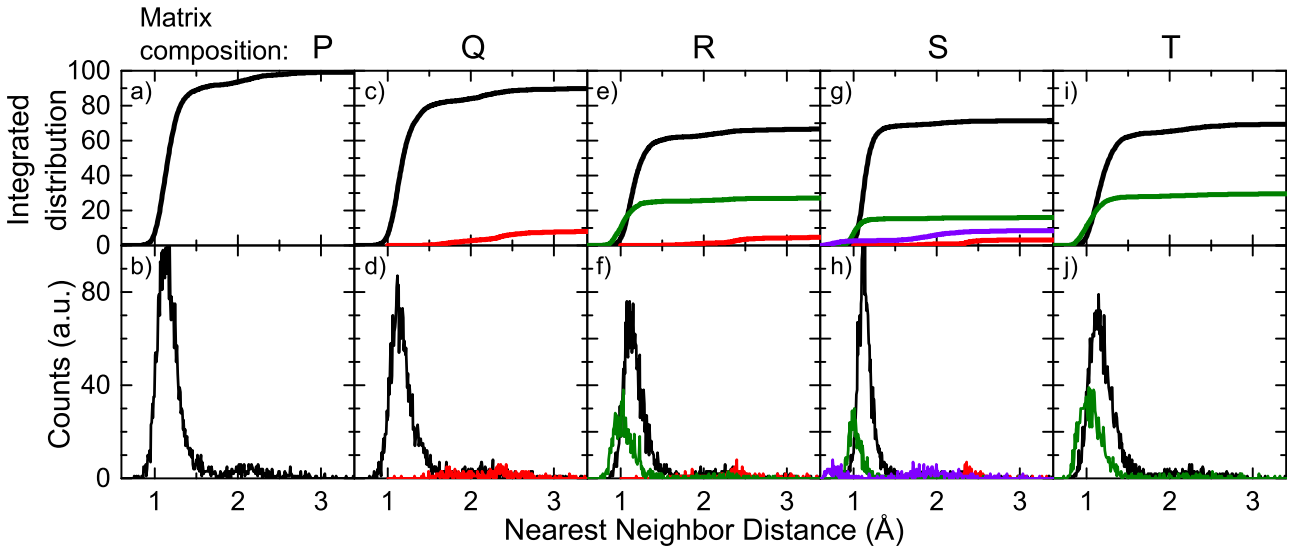

FIG. 8. Distribution of nearest neighbors. Calculation of the final rest location of the projectile deuterium in relationship to other elements in the matrix was performed with 5004 random trajectories per matrix. The distance (horizontal axis) of nearest neighbor species to retained deuterium, within the simulation matrix following D-atom bombardment, is used to indicate the frequency of elemental binding pairs. The deuterium bombardment was conducted in the five different matrix compositions P, Q, R, S, and T. The distances from deuterium to carbon are shown in black, to lithium in red, to oxygen in green, and to sample-preloaded deuterium in purple. The top panes represent the integrated distributions of the nearest neighbors, shown in the bottom panes.

as their nearest neighbor 30% of the time. Importantly, if the matrix is prepared with "cumulated" deuterium so that Li, O, and D have the same, 16%, atomic fraction in carbon, case S, the qualitative conclusions are the same.

In Figures 8(c) and 8(d), the sample matrix contains 20% lithium and 80% carbon; after deuterium bombardment, less than 10% of the implanted deuterium finds lithium as its nearest neighbor. The case where the carbon matrix contains both 20% lithium and oxygen (e,f) also shows that deuterium has ~30% oxygen as its nearest neighbor with minimal lithium nearest neighbors. Thus, even when lithium is present in the carbon matrix, deuterium preferentially chooses the vicinity of oxygen for its final bonding. This result corroborates the XPS spectral shifts correlated to the presence of lithium and deuterium where the effect is predominantly in the electronic band states of oxygen atoms after irradiation with D ions.

Figures 9(a)–9(d) show the post D bombardment average distributions of charges of all atoms in the matrix, which corroborate the conclusion in Figures 7 and 8. These matrix atoms include only those cases where D was retained. The surfaces of amorphous carbon (a-C) as well as a-C:Li/O with various concentrations of Li and O are considered. The distributions of charges in the bottom panels of Figure 9 for C,

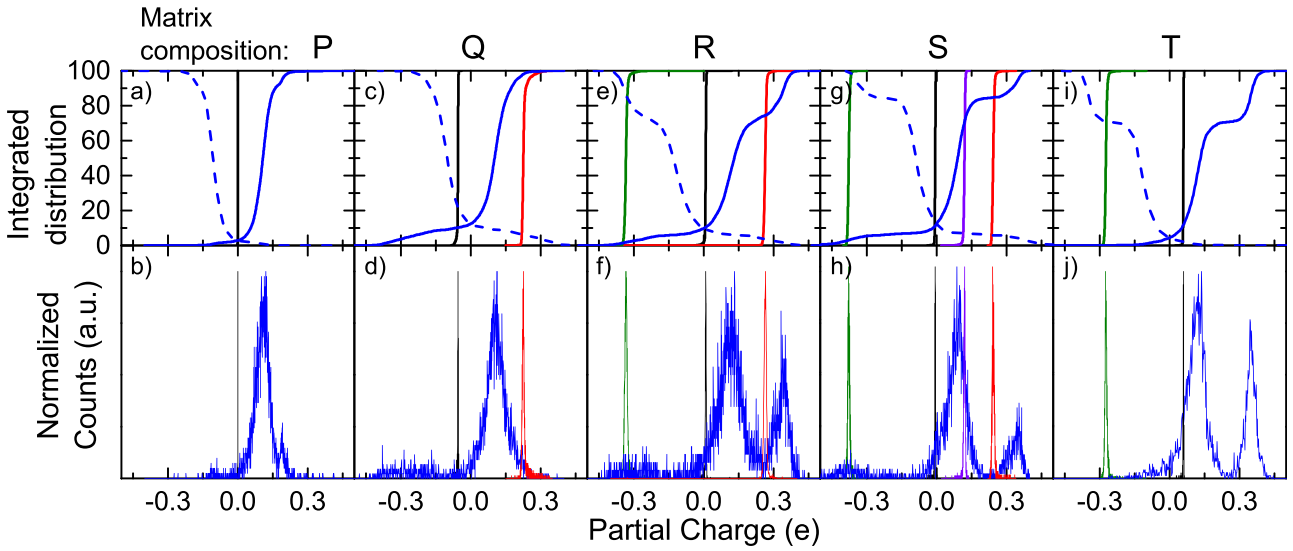

FIG. 9. Distribution of charges following D bombardment by 5004 independent random trajectories. The top panes represent the normalized integrated distribution of charges shown in the bottom panes. The species charge distribution within the simulation matrix following deuterium bombardment is used to easily identify the strength of the elemental binding pairs. Contributions from carbon are shown in black, lithium in red, oxygen in green, sample-preloaded with hydrogen in purple, and impacting deuterium in blue. For convenience in showing what species neutralize deuterium, the deuterium-integrated distribution is also shown flipped (dashed lines), where the x-axis is multiplied by −1.

Li, and O (the atoms in the target cell) were calculated as the average charge of all atoms of a particular element in the final instant of time for each trajectory, resulting in one value for each of C, Li, and O per trajectory. The charges of the target-cell atoms change mainly for those atoms that are along the trajectory of impact D, and this effect is well amortized by the averaging over the whole cell, leading in sharp peaks of the C, Li and O distributions. However, since there is no averaging of charges over impact D (there is only one D per trajectory) the charge distributions of D reflect the actual (non-averaged) partial charges of the impinging D, which may significantly vary from trajectory to trajectory, explaining why the charge distributions for D are much wider than those of the target atoms.

The top panes in Figure 9 show the integrated and normalized charge distributions of the bottom panes. The impacting D adapts to the charges of the target, in particular at its bonding site, so its partial charge neutralization indicates to what atom(s) it is bonding, keeping the system quasi-neutral (within numerical error). For that reason, in order to see which matrix atom (i.e., carbon, oxygen, or lithium) neutralizes the incident deuterium ion, the integral distribution of charges of the impacting D is shown multiplied by −1 (negative-one). Thus, in (f), oxygen at −0.33 e is neutralizing the deuterium at +0.34 e, lithium at +0.26 e neutralizes the small deuterium peak at −0.26 e, and the remaining deuterium at +0.1 e is counterpoised by the highly neutral carbon. Panes (e-f) quantitatively show the neutralizing effect of lithium and oxygen together. Oxygen neutralizes ∼25%, carbon neutralizes ∼68% of the deuterium, and lithium is responsible for ∼7% deuterium neutralization. The partial charges analysis is indicative of the underlying chemistry. Thus, as seen in (c-d), where only 20% of Li is mixed with carbon, by comparison with (a-b) containing only C, it follows that less than 15% of D atoms are interacting with Li atoms or Li-C compounds. But Figures 9(i) and 9(j), where the sample is loaded with 20% O in carbon and *no lithium*, shows that about 30% of D is neutralizing O and even more by C-O compounds. The role of oxygen is even more strongly confirmed in the case shown in Figures 9(e) and 9(f) where there is an equivalent, 20% concentrations of O and Li in the carbon. Apart from the less than 10% of D that is bound to Li-C, about 40% is interacting with O or C-O compounds, indicating that when there is a sufficient amount of oxygen, the chemistry of the retained D is dominated by the presence of oxygen rather than lithium.

Interestingly, the recent *ab initio* computational chemistry calculations[39,40] using Plane-Wave DFT to study the binding chemistry of H, O, and Li with a graphene matrix are consistent with our conclusions obtained here by the quantum-classical molecular dynamics of a lithiated and oxidized amorphous carbon slab. Thus, it is found that the addition of lithium to the oxygenated graphite surface does not improve the hydrogen retention, while various combinations of single vacancy and oxygen atoms give rise to very powerful attractive centers for H, which is not improved by adding Li. On the other hand, when only Li is present in the graphite surface it does reinforce to some extent the H bonding to the graphite, consistent with conclusions in Ref. 28, where calculations were done with only 6% oxygen in the surface sample. However, as shown in Ref. 14, when only Li is present in graphite, the graphite erosion increases and D uptake does not significantly increase. The expected behavior of increased D uptake and suppressed chemical sputtering of carbon is only obtained when oxygen is present in the sample in quantities comparable to these of lithium (∼20%). As our experiments show, these quantities are readily achieved in the lithiated graphite surface upon D bombardment.

IV. CONCLUSIONS

Lithium is used in a wide variety of systems due to its unique interactions with hydrogen, and its use in fusion devices has dramatically improved plasma performance through enhanced deuterium particle control. Initially, these improvements were suspected to be a result of direct LiD bonding. The present work builds on our previous results[14] and demonstrates how the oxygen surface concentration in lithiated graphite evolves with respect to the time after deposition, lithium dose, and deuterium fluence.

The oxygen surface concentration slowly but consistently increases after lithium deposition as the lithiated graphite sample sits in UHV. Over the course of ∼100 h, the oxygen surface concentration increases from 5% to 20%. We also found that the oxygen surface concentration increases rapidly as deuterium fluence increases. Lithium dose, without subsequent irradiation, however, does not directly influence the prompt oxygen concentration. We conjecture that this is because the sample surface area dominates the oxygen gettering rate, as opposed to the lithium dose.

Throughout the experimental section of the present work, oxygen is found to play a consistent and dynamic role in lithiated graphite. This role is accentuated after deuterium irradiation, as manifest by the dramatic increase in the oxygen surface concentration. Atomistic simulations corroborate the experimental results and further define the role of oxygen in retaining deuterium. "Partial charges" and "nearest neighbors" analyses from the simulations show that implanted 5 eV deuterium preferentially neutralizes with and comes to rest near oxygen rather than lithium, thus indicating deuterium-oxygen bonding. This preferential interaction reveals that deuterium-oxygen bonding is the primary mechanism for deuterium retention in lithiated graphite.

ACKNOWLEDGMENTS

C.N.T. and J.P.A. acknowledge financial support by U.S. DOE Contract No. DE-FG02-08ER54990. P.S.K. acknowledges support of the U.S. DOE, Office of Fusion Energy Sciences, and (P.S.K. and J.D.) the LDRD program of the Oak Ridge National Laboratory. The computed data were obtained at the DOE computational resources of the NCCS (Jaguar) and at NSF computational resources of the NICS (Kraken). P.S.K. and J.D. acknowledge computer support of the DOE INCITE program and NSF Xsede program. C.S. acknowledges support from US DOE Contract No. DE AC02-09CH11466.

[1]D. C. Elias, R. R. Nair, T. Mohiuddin, S. V. Morozov, P. Blake, M. P. Halsall, A. C. Ferrari, D. W. Boukhvalov, M. I. Katsnelson, and A. K. Geim, Science **323**, 610 (2009).
[2]T. Zheng, J. S. Xue, and J. R. Dahn, Chem. Mater. **8**, 389 (1996).
[3]D. W. Boukhvalov and C. Virojanadara, Nanoscale **4**, 1749 (2012).
[4]M. Ono, M. G. Bell, Y. Hirooka, R. Kaita, H. W. Kugel, G. Mazzitelli, J. E. Menard, S. V. Mirnov, M. Shimada, C. H. Skinner, and F. L. Tabarés, Nucl. Fusion **52**, 037001 (2012).
[5]M. Ono, M. A. Jaworski, R. Kaita, H. W. Kugel, J. W. Ahn, J. P. Allain, M. G. Bell, R. E. Bell, D. J. Clayton, J. M. Canik, S. Ding, S. Gerhardt, T. K. Gray, W. Guttenfelder, Y. Hirooka, J. Kallman, S. kaye, D. Kumar, B. P. LeBlanc, R. Maingi, D. K. Mansfield, A. Mclean, J. Menard, D. Mueller, R. Nygren, S. Paul, M. Podesta, R. Raman, Y. Ren, S. Sabbagh, F. Scotti, C. H. Skinner, V. A. Soukhanovskii, V. Surla, C. N. Taylor, J. Timberlake, and L. E. Zakharov, and NSTX Research Team, Nucl. Fusion **53**, 113030 (2013).
[6]J. Hemminger, G. R. Fleming, and M. A. Ratner, Directing Matter and Energy: Five Challenges for Science and the Imagination A Report from the Basic Energy Sciences Advisory Committee December 20, 2007.
[7]D. K. Mansfield, K. W. Hill, J. D. Strachan, M. G. Bell, S. D. Scott, R. Budny, E. S. Marmar, J. A. Snipes, J. L. Terry, and S. Batha, Phys. Plasmas **3**, 1892 (1996).
[8]R. Majeski, M. Boaz, D. Hoffman, B. Jones, R. Kaita, H. Kugel, T. Munsat, J. Spaleta, V. A. Soukhanovskii, J. Timberlake, L. Zakharov, G. Antar, R. P. Doerner, S. Luckhardt, R. W. Conn, M. Finkenthal, D. Stutman, R. Maingi, and M. Ulrickson, Fusion Eng. Des. **65**, 443 (2003).
[9]A. A. Tuccillo, A. Alekseyev, B. Angelini, S. V. Annibaldi, M. L. Apicella, G. Apruzzese, J. Berrino, E. Barbato, A. Bertocchi, A. Biancalani, W. Bin, A. Botrugno, G. Bracco, S. Briguglio, A. Bruschi, P. Buratti, G. Calabrò, A. Cardinali, C. Castaldo, C. Centioli, R. Cesario, L. Chen, S. Cirant, V. Cocilovo, F. Crisanti, R. De Angelis, U. de Angelis, L. Di Matteo, C. Di Troia, B. Esposito, G. Fogaccia, D. Frigione, L. Gabellieri, F. Gandini, E. Giovannozzi, G. Granucci, F. Gravanti, G. Grossetti, G. Grosso, F. Iannone, H. Kroegler, V. Lazarev, E. Lazzaro, I. E. Lyublinski, G. Maddaluno, M. Marinucci, D. Marocco, J. R. Martin-Solis, G. Mazzitelli, C. Mazzotta, V. Mellera, F. Mirizzi, S. Mirnov, G. Monari, A. Moro, V. Muzzini, S. Nowak, F. P. Orsitto, L. Panaccione, D. Pacella, M. Panella, F. Pegoraro, V. Pericoli-Ridolfini, S. Podda, S. Ratynskaia, G. Ravera, A. Romano, A. Rufoloni, A. Simonetto, P. Smeulders, C. Sozzi, E. Sternini, B. Tilia, O. Tudisco, A. Vertkov, V. Vitale, G. Vlad, R. Zagórski, M. Zerbini, and F. Zonca, Nucl. Fusion **49**, 104013 (2009).
[10]J. Sánchez, F. L. Tabarés, D. Tafalla, J. A. Ferreira, I. García-Cortés, C. Hidalgo, F. Medina, M. A. Ochando, M. A. Pedrosa, and T. T.-I. Team, J. Nucl. Mater. **390–391**, 852–857 (2009).
[11]S. V. Mirnov, V. B. Lazarev, S. M. Sotnikov, V. A. Evtikhin, I. E. Lyublinski, and A. V. Vertkov, Fusion Eng. Des. **65**, 455 (2003).
[12]G. S. Xu, B. N. Wan, J. G. Li, X. Z. Gong, J. S. Hu, J. F. Shan, H. Li, D. K. Mansfield, D. A. Humphreys, V. Naulin, and International Collaborators, Nucl. Fusion **51**, 072001 (2011).
[13]M. J. Baldwin, R. P. Doerner, S. C. Luckhardt, and R. W. Conn, Nucl. Fusion **42**, 1318 (2002).
[14]P. S. Krstic, J. P. Allain, C. N. Taylor, J. Dadras, S. Maeda, K. Morokuma, J. Jakowski, A. Allouche, and C. H. Skinner, Phys. Rev. Lett. **110**, 105001 (2013).
[15]D. Ensling, A. Thissen, and W. Jaegermann, Scr. Mater. **255**, 2517 (2008).
[16]S. S. Harilal, J. P. Allain, A. Hassanein, M. R. Hendricks, and M. Nieto-Perez, Appl. Surf. Sci. **255**, 8539 (2009).
[17]C. N. Taylor, B. Heim, and J. P. Allain, J. Appl. Phys. **109**, 053306 (2011).
[18]H. Estrade-Szwarckopf and B. Rousseau, Synth. Met. **23**, 191 (1988).
[19]N. Itou, H. Toyoda, K. Morita, and H. Sugai, J. Nucl. Mater. **290–293**, 281 (2001).
[20]S. Kato, M. Watanabe, H. Toyoda, and H. Sugai, J. Nucl. Mater. **266–269**, 406 (1999).
[21]C. N. Taylor, J. P. Allain, B. Heim, P. S. Krstic, C. H. Skinner, and H. W. Kugel, J. Nucl. Mater. **415**, S777 (2011).
[22]O. El-Atwani, J. P. Allain, and S. Ortoleva, Nucl. Instrum. Methods Phys. Res. B **272**, 210 (2012).
[23]C. N. Taylor, B. Heim, S. Gonderman, J. P. Allain, Z. Yang, R. Kaita, A. L. Roquemore, C. H. Skinner, and R. A. Ellis, Rev. Sci. Instrum. **83**, 10D703 (2012).
[24]J. H. Scofield, *Theoretical Photoionization Cross Sections From 1 to 1500 keV* (Lawrence Livermore Laboratory, 1973).
[25]L. Pauling, *The Nature of the Chemical Bond and the Structure of Molecules and Crystals: An Introduction to Modern Structural Chemistry*, 3rd ed. (Cornell University Press, 1960).
[26]H. Sugai, M. Ohori, and H. Toyoda, Vacuum **47**, 981 (1996).
[27]H. Sugai, H. Toyoda, K. Nakamura, K. Furuta, M. Ohori, K. Toi, S. Hirokura, and K. Sato, J. Nucl. Mater. **220–222**, 254 (1995).
[28]P. S. Krstic, J. P. Allain, A. Allouche, J. Jakowski, J. Dadras, C. N. Taylor, Z. Yang, K. Morokuma, and S. Maeda, Fusion Eng. Des. **87**, 1732 (2012).
[29]C. H. Skinner, R. Sullenberger, B. E. Koel, M. A. Jaworski, and H. W. Kugel, J. Nucl. Mater. **438**, S647 (2013).
[30]J. R. Hoenigman and R. G. Keil, Appl. Surf. Sci. **18**, 207 (1984).
[31]D. den Engelsen and B. Ferrario, J. Vac. Sci. Technol. B **22**, 809 (2004).
[32]A. Khan,"Surface characterization of lithiumized plasma-facing components for fusion reactors," Senior thesis (Princeton University, 2012).
[33]Y. Cong and Z.-Z. Yang, Chem. Phys. Lett. **316**, 324 (2000).
[34]P. S. Krstic, C. O. Reinhold, and S. J. Stuart, New J. Phys. **9**, 209 (2007).
[35]P. S. Krstic, R. J. Harrison, and B. G. Sumpter, Phys. Scr. **T124**, 101 (2006).
[36]M. Elstner, D. Porezag, G. Jungnickel, J. Elsner, M. Haugk, T. Frauenheim, S. Suhai, and G. Seifert, Phys. Rev. B **58**, 7260 (1998).
[37]G. Zheng, M. Lundberg, J. Jakowski, T. Vreven, M. J. Frisch, and K. Morokuma, Int. J. Quantum Chem. **109**, 1841 (2009).
[38]C. H. Skinner, J. P. Allain, W. Blanchard, H. W. Kugel, R. Maingi, A. L. Roquemore, V. A. Soukhanovskii, and C. N. Taylor, J. Nucl. Mater. **415**, S773 (2011).
[39]A. Allouche and P. S. Krstic, Carbon **50**, 510 (2012).
[40]A. Allouche and P. S. Krstic, Carbon **50**, 3882 (2012).